

The QCD phase diagram according to the center group

Ydalia Delgado Mercado^a, Hans Gerd Evertz^b, Christof Gattringer^a

^a*Institut für Physik, Karl-Franzens Universität, Graz, Austria*

^b*Institute for Theoretical and Computational Physics, Technische Universität Graz, Austria*

We study an effective theory for QCD at finite temperature and density which contains the leading center symmetric and center symmetry breaking terms. The effective theory is studied in a flux representation where the complex phase problem is absent and the model becomes accessible to Monte Carlo techniques also at finite chemical potential. We simulate the system using a generalized Prokof'ev-Svistunov worm algorithm and compare the results to a low temperature expansion. The phase diagram is determined as a function of temperature, chemical potential and quark mass. Shape and quark mass dependence of the phase boundaries are as expected for QCD. The transition into the deconfined phase is smooth throughout, without any discontinuities or critical points.

PACS numbers: 12.38.Aw, 11.15.Ha, 11.10.Wx

Obtaining a deeper understanding of the QCD phase diagram will be one of the central goals of particle physics in the coming years. With running and upcoming experiments that drive this development, also the theoretical side is challenged to improve our understanding of the QCD phase structure. Analyzing phase transitions is clearly a non-perturbative problem and suitable techniques have to be applied. For vanishing chemical potential, lattice QCD is a powerful method that provides reliable quantitative information on the QCD finite temperature transition. However, for non-vanishing density the notorious complex phase problem so far limits numerical lattice QCD studies to painfully small volumes.

For quenched QCD, where the quark contributions to the path integral are neglected, the deconfinement transition is related to the center group \mathbb{Z}_3 of $SU(3)$, which is a symmetry in the confined low temperature phase, while it is broken spontaneously above the deconfinement temperature [1]. When one couples the dynamics of the quark fields, the center symmetry is broken explicitly by the fermion determinant. This explicit breaking overlays the spontaneous breaking of the quenched theory. However, as for spin systems, one may expect that also for QCD the underlying symmetry still governs parts of the dynamics of the full theory, e.g., via the center properties of canonical determinants [2].

In order to study the role of center symmetry for the QCD phase diagram, we here analyze an effective theory which contains the leading center symmetric and center symmetry breaking terms. This *effective center theory* can be mapped exactly to a flux representation [3], where the complex phase problem is absent. So far the model was studied only in a very limited parameter range [3–7]. Here we apply a generalization of the worm algorithm [8] which allows us to efficiently explore the full range of temperatures and chemical potential values. This constitutes one of the very few examples where a QCD related complex phase problem can be solved. We study the phase diagram of the effective center theory and analyze what role the center degrees of freedom of QCD play for the phase structure of hot and dense matter.

Effective center theory and flux representation

The effective center theory is defined by the action [3]

$$S[P] = -\sum_x \left(\tau \sum_{\nu=1}^3 \left[P_x P_{x+\hat{\nu}}^* + c.c. \right] + \eta P_x + \bar{\eta} P_x^* \right). \quad (1)$$

The dynamical degrees of freedom are the center variables $P_x \in \mathbb{Z}_3 = \{1, e^{i2\pi/3}, e^{-i2\pi/3}\}$ at the sites x of a 3-dimensional cubic lattice. The partition function is a sum over all configurations of the center variables, $Z = \sum_{\{P\}} \exp(-S[P])$. The first term of the action (1) is a nearest neighbor interaction which is invariant under global center transformations ($P_x \rightarrow z P_x$), where all variables are transformed with a center element $z \in \mathbb{Z}_3$. The form of this term may be obtained from a strong coupling expansion of the effective action for the Polaykov loop which in quenched QCD is the order parameter for center symmetry and for confinement. The variables P_x take over the role of the local Polyakov loops. Although in full QCD center symmetry is broken explicitly by the quarks, the Polyakov loop is still used to monitor confinement properties and to determine the crossover temperature (see, e.g., [9, 10]). The strong coupling expansion also identifies the parameter τ as an increasing function of the temperature T of the underlying lattice QCD theory, and for brevity we refer to τ as *temperature*.

The second term of the effective action may be obtained from a hopping (i.e., large quark mass) expansion of the fermion determinant and contains the leading center symmetry breaking contributions. The parameters $\eta = \kappa e^\mu$, $\bar{\eta} = \kappa e^{-\mu}$ are related to the chemical potential μ . The hopping expansion shows that $\kappa = N_f h(m)$, where N_f is the number of flavors and $h(m)$ is a function of the QCD quark mass m which decreases with increasing m . We refer to κ as the *inverse mass parameter*.

For vanishing external field, $\kappa = 0$, the model reduces to the 3-state Potts model, which is known to have a first order transition at $\tau = 0.183522(3)$ [11]. For small external field κ and vanishing μ the first order transition persists, giving rise to a short first order line which terminates at a critical endpoint at $(\tau, \kappa) =$

(0.183127(7), 0.00026(3)) [11]. For small non-zero μ the system has been analyzed with techniques based on the Swendsen-Wang cluster algorithm [4], with reweighting [5] and with imaginary μ [6]. Within the flux representation [3] local Metropolis updates were also used [3, 4, 7]. It has been demonstrated that turning on the chemical potential softens the transition and shifts the critical end-point towards smaller values of κ . So far no simulations were done in the parameter region where the complex phase problem of the formulation (1) becomes severe (see [4] for a discussion of that regime).

The flux representation [3] solves the complex phase problem. We briefly summarize it to discuss our observables and conventions: The Boltzmann factors for the nearest neighbor terms of (1) can be rewritten as

$$e^{\tau[P_x P_{x+\hat{\nu}}^* + c.c.]} = C \sum_{b_{x,\nu}=-1}^{+1} B^{|b_{x,\nu}|} (P_x P_{x+\hat{\nu}}^*)^{b_{x,\nu}}. \quad (2)$$

The sum on the right hand side is over *flux variables* $b_{x,\nu} \in \{-1, 0, +1\}$ attached to the links of the lattice. The constants C and B depend on the temperature τ via $C = (e^{2\tau} + 2e^{-\tau})/3$ and $B = (e^{2\tau} - e^{-\tau})/3C$. Similarly one expresses the center symmetry breaking terms as

$$e^{\eta P_x + \bar{\eta} P_x^*} = \sum_{s_x=-1}^{+1} M_{s_x} P_x^{s_x}, \quad (3)$$

where we sum over *monomer variables* $s_x \in \{-1, 0, +1\}$ attached to the sites x . It is straightforward to work out the monomer weights M_s for $s = -1, 0, +1$,

$$M_s = \frac{1}{3} \left[e^{\eta + \bar{\eta}} + 2e^{-(\eta + \bar{\eta})/2} \cos \left(\frac{\sqrt{3}}{2}(\eta - \bar{\eta}) - s \frac{2\pi}{3} \right) \right]. \quad (4)$$

The weights M_s turn out to be non-negative.

Inserting (2) and (3) into the partition sum gives rise to a complete factorization of the dependence on the dynamical variables P_x and the sum over all configurations can be performed. One ends up with a new form for the partition sum (we drop an irrelevant overall constant),

$$Z = \sum_{\{b,s\}} W(b,s) \prod_x T \left(\sum_{\nu} [b_{x,\nu} - b_{x-\hat{\nu},\nu}] + s_x \right). \quad (5)$$

The partition function is now a sum over configurations $\{b,s\}$ of the flux and monomer variables. Each configuration comes with a real non-negative weight factor $W(b,s) = (\prod_{x,\nu} B^{|b_{x,\nu}|}) (\prod_x M_{s_x})$. For every link with non-vanishing flux, i.e., $b_{x,\nu} = \pm 1$, a factor B is taken into account. Sites x contribute with factors M_{s_x} according to their monomer values $s_x \in \{-1, 0, +1\}$.

The flux/monomer configurations are subject to constraints: In (5) $T(n)$ is the triality function defined as $T(n) = \delta_{n \bmod 3, 0}$. The constraints enforce that at every site x the total flux from both, flux variables $b_{x,\nu}$ and monomers s_x , is a multiple of 3. In the flux form (5) the partition sum contains only real and non-negative contributions and thus the complex phase problem is solved.

In this letter we focus on bulk observables such as the order parameter P and the corresponding susceptibility, which both are obtained as derivatives of the free energy, $\langle P \rangle = \partial \ln Z / \partial \eta$ and $\chi_P = \partial^2 \ln Z / \partial \eta^2$. In a similar way one obtains the internal energy U and the heat capacity C . For an efficient evaluation the identities $\partial M_{+1} / \partial \eta = M_0$, $\partial M_0 / \partial \eta = M_{-1}$ and $\partial M_{-1} / \partial \eta = M_{+1}$ are useful. In the end all our observables are expressed in terms of the total flux and monomer numbers and their moments.

Simulation with the worm algorithm

Having established the flux representation where the complex phase problem is solved, we now must find a suitable algorithm for an efficient Monte Carlo update. We here use a generalized form of the Prokof'ev-Svistunov worm algorithm [8]: The worm starts at a randomly chosen site and moves along links until it returns to the starting point where it terminates. We allow for two different moves of our worm: A) The worm randomly chooses a new direction at a site and changes the flux at the corresponding link by ± 1 . B) The worm decides to change a monomer variable by ± 1 and then randomly hops to another site where the monomer variable is changed by ∓ 1 . The moves are offered with equal probability, produce only configurations that are compatible with the constraint, and lead to an ergodic algorithm. The Metropolis acceptance probabilities are $p_A = B^{\delta_b}$ when changing a flux variable b by an amount of δ_b (Move A), and $p_B = M_{s'}/M_s$ for changing a monomer variable from s to s' (Move B). A more complete account of the algorithm and its implementation will be given elsewhere.

We generated ensembles for lattice sizes 36^3 , 48^3 , 64^3 and 72^3 . For the inverse mass parameter we used $\kappa = 0.1, \kappa = 0.01, \kappa = 0.005$ and $\kappa = 0.001$. The evaluation of our observables $\langle P \rangle$, χ_P , U and C is based on up to 10^6 configurations, separated by 10 worms for decorrelation. Autocorrelation times were determined and used in the estimate for the statistical errors. Finite volume effects were analyzed by comparing the different system sizes and are negligible for our final results.

The results from the new worm algorithm were checked using several strategies. For vanishing inverse mass parameter the known results [11] for the 3-state Potts model with external magnetic field were reproduced. For small values of τ and arbitrary κ and μ we used low temperature expansion techniques to determine the power series for the partition sum, taking into account all terms up to τ^3 . For small τ we found excellent agreement between the Monte Carlo results and the perturbative series (see Fig. 2). Finally, for all our production and analysis codes two independent programs were written for cross checks.

Results from the Monte Carlo calculation

We begin the discussion of our results with the order parameter $\langle P \rangle$, which – as discussed above – is identified with the Polyakov loop of QCD. In Fig. 1 we show the results for $\langle P \rangle / V$ as a function of τ and μ for our 36^3 ensembles at $\kappa = 0.01$. For roughly 450 points in the

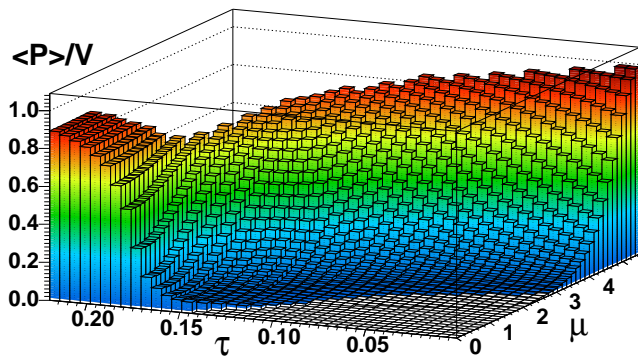


FIG. 1: The order parameter $\langle P \rangle/V$ as a function of temperature τ and chemical potential μ from our 36^3 , $\kappa = 0.01$ ensembles. Near the rear left corner no data were computed. $\langle P \rangle/V$ has values close to 1 there. For small τ and μ the order parameter approaches 0.

τ - μ plane the values of $\langle P \rangle/V$ were evaluated and used for the 3-D plot. In the rear left corner and for small τ and μ no data were computed. $\langle P \rangle/V$ is expected to be close to 1 in the rear left corner. For small τ and μ there is a sizable region where the expectation value $\langle P \rangle/V$ is small and center symmetry is broken only very mildly. Transferring this finding from the effective center theory to QCD implies that for small temperature and density, matter is confined. When τ or μ are increased, the system undergoes a change and $\langle P \rangle/V$ reaches values close to 1. For QCD this implies that both temperature and μ may be used to drive the system into the deconfined phase characterized by a large Polyakov loop.

The next step in the analysis of the phase diagram is to identify the phase boundary. For that purpose we studied the susceptibility χ_P and the heat capacity C as a function of μ at fixed τ (symbols with horizontal error bars in Figs. 2 and 3) or as a function of τ at fixed μ (vertical error bars) and determined the position of the maximum: We fitted the data for χ_P and C near the maxima with a parabola and obtained the position of the maximum as one of the fit parameters. The corresponding statistical error was computed with the jackknife method. In Fig. 2 we show the positions of the maxima of χ_P in the τ - μ plane. We compare the results for 4 values of the inverse mass parameter κ and connect the data at the same κ with a dotted line to guide the eye. The dashed horizontal line at the top marks the value of the critical τ for the 3-state Potts model, i.e., the situation at $\kappa = 0$. The dashed curves near the bottom of the plot are the results from the perturbative series for small τ which we briefly discussed in the last section. The Monte Carlo data nicely approach these curves for $\tau \rightarrow 0$.

The curves in Fig. 2 separate the phases with small order parameter and with $\langle P \rangle/V \sim 1$, i.e., the confined and the deconfined phases. The phase boundaries depend on the inverse mass parameter κ , and their behavior is as expected for QCD: The intercept of the phase lines with the μ -axis shifts to the left with decreasing quark mass (i.e., increasing inverse mass parameter κ) because a smaller chemical potential is sufficient to excite lighter states.

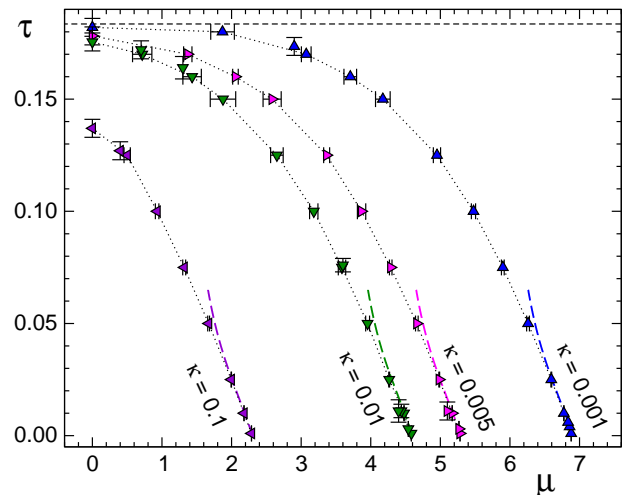


FIG. 2: Phase diagram as obtained from the maxima of the Polyakov loop susceptibility χ_P . We show results at 4 values of the inverse mass parameter κ . The dashed curves at the bottom are the results of the τ expansion and the horizontal line marks the critical value of τ for the $\kappa = 0$ case.

Also the intercept with the τ -axis drops with increasing κ , corresponding to the fact that for quenched QCD (i.e., infinite quark mass) the transition temperature is considerably higher than the crossover temperature of QCD with physical quark masses. The mass dependence of the phase boundaries thus is as expected for QCD.

A key problem of the QCD phase diagram is the question about the nature of the various transitions and phases. Unless one goes to very high densities where more exotic phases exist, two principal phases are expected. A phase with conventional matter (confined with broken chiral symmetry) and a plasma phase (deconfined and chirally symmetric). In some parameter regions also a quarkyonic phase with confinement but restored chiral symmetry has been discussed. For the transition lines a standard scenario is that at $\mu = 0$ for physical quark masses the finite temperature transition is merely a crossover [12], where different second derivatives of the free energy peak at different temperature values [9, 10]. With increasing μ the crossover region narrows and terminates at a critical endpoint. From the endpoint on a first order transition line continues (which at some point might hit other transitions to the exotic phases mentioned). Alternative scenarios suggest that either no critical endpoint appears and crossover type of behavior persists also for large μ and low temperature, or that even more than one endpoint might exist. For a glimpse of the current debate see e.g. [13].

While we cannot address questions concerning chiral symmetry in the effective center theory, we can analyze the type of transitions that take place at the phase boundaries. To determine the nature of the transitions we used two techniques. We analyzed histograms for the distribution of the order parameter and the action near the phase boundaries. For a first order transition the histograms would display a double peak structure near

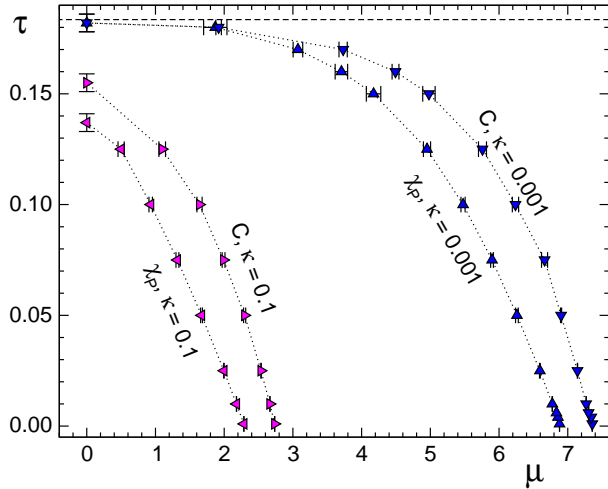


FIG. 3: Comparison of the phase boundaries obtained from the maxima of susceptibility χ_P and heat capacity C .

the critical line. In our analysis we found only single peaks and thus rule out first order behavior. The second approach is a comparison of the normalized susceptibilities and heat capacities χ_P/V and C/V from lattices with different volumes. For a first order transition the height of the maxima diverges proportional to V , while for a continuous transition the divergence is modified by a critical exponent. A height which is independent of V indicates a smooth crossover. Our analysis shows that for the phase boundaries of Figs. 2 and 3 the height is independent of V for all volumes we studied. We conclude that the transitions in the effective center theory are smooth crossover lines.

Once the crossover nature is established, one may ask how wide the transition region is – similar to the finite temperature crossover of QCD at zero density, which is 20 - 30 MeV wide. In order to get an estimate for the width of the crossover region, in Fig. 3 we compare the positions of the maxima of the susceptibility χ_P and of the heat capacity C for two values of κ . The fact that the corresponding lines do not coincide stresses again the crossover nature of the transition, and the plot demonstrates that the crossover region is rather wide for most of the parameter values. Only for small κ and μ the lines approach each other, anticipating the first order behavior which is known for very small κ and μ [4, 5].

Concluding remarks

In this letter we report on our results for the phase diagram of an effective theory for the center degrees of freedom of QCD. Using the flux representation solves the complex phase problem and we develop a generalized worm algorithm for a Monte Carlo calculation in a wide range of temperatures and chemical potential.

The outcome of our analysis is a version of the QCD phase diagram when only the center degrees of freedom are considered. The phase diagram shares many features with the conjectured full QCD phase diagram: The transition to the deconfined phase can be driven by both, temperature or μ , and the quark mass dependence is as expected for QCD. The phase boundaries between a phase with only very small center symmetry breaking ($\langle P \rangle/V \sim 0$) and a phase with $\langle P \rangle/V \sim 1$ has a shape which is similar to the one conjectured for QCD. For all parameter values we studied, the transition is of a smooth crossover type and we conclude that center symmetry alone does not provide a mechanism for possible first order behavior in the QCD phase diagram.

Various future research directions may be followed: The effective theory can be made more realistic by replacing the \mathbb{Z}_3 spins by continuous $SU(3)$ valued variables (here some work is in progress and also for this theory the complex phase problem can be solved by a suitable flux representation). Furthermore it would be desirable to take into account also the fermion nature of the problem – an aspect which is absent in the current effective action. Another interesting direction is of a more technical nature: With our effective theory we have a reference example of a QCD related system where the complex action problem is solved. This reference theory can and should be used to test the reliability and limitations of various techniques for QCD with chemical potential, such as reweighting, series expansions or complex Langevin methods.

Acknowledgments

The authors thank P. de Forcrand, C.B. Lang, R. Ritter, B.-J. Schaefer and U.-J. Wiese for valuable discussions and remarks. The project has been supported by FWF DK 1203 and Marie Curie ITN STRONGnet.

-
- [1] L. McLerran, B. Svetitsky, Phys. Rev. D **24**, 450 (1981). L.G. Yaffe, B. Svetitsky, Phys. Rev. D **26** (1982) 963; Nucl. Phys. B **210** 423. A.M. Polyakov, Phys. Lett. B **72** (1978) 477. L. Susskind, Phys. Rev. D **20** (1979) 2610.
 - [2] E. Bilgici *et al*, Phys. Lett. B. **697** (2011) 85.
 - [3] A. Patel, Nucl. Phys. B **243** (1984) 411; Phys. Lett. B **139** (1984) 394. T. DeGrand, C. DeTar, Nucl. Phys. B **225** (1983) 590. C. Bernard *et al.*, Phys. Rev. D **49** (1994) 6051.
 - [4] M.G. Alford, S. Chandrasekharan, J. Cox, U.-J. Wiese, Nucl. Phys. B **602** (2001) 61.
 - [5] S. Kim, P. de Forcrand, S. Kratochvila, T. Takaishi, PoS **LAT2005** (2006) 166.
 - [6] P. de Forcrand, O. Philipsen, Phys. Rev. Lett. **105** (2010) 152001.
 - [7] J. Condella, C. DeTar, Phys. Rev. D **61** (2000) 074023.
 - [8] N. Prokof'ev, B. Svistunov, Phys. Rev. Lett. **87** (2001) 160601.
 - [9] S. Borsanyi *et al.*, JHEP **1009** (2010) 073.
 - [10] A. Bazavov *et al.* [HotQCD], [arXiv:1009.4914 [hep-lat]].

- [11] R.V. Gavai, F. Karsch, B. Petersson, Nucl. Phys. B **322** (1989) 738. W. Janke, R. Villanova, Nucl. Phys. B **489** (1997) 679, and references therein. F. Karsch and S. Stickan, Phys. Lett. B **488** (2000) 319.
- [12] Y. Aoki *et al.*, Nature **443** (2006) 675.
- [13] K. Fukushima, T. Hatsuda, Rep. Prog. Phys. **74** (2011) 014001. P. Braun-Munzinger, J. Wambach, Rev. Mod. Phys. **81** (2009) 1031.